www.acsnano.org

Crea Sem in P Madisen Mei-Yin

Creating a Nanoscale Lateral Junction in a Semiconductor Monolayer with a Large Built in Potential

Madisen Holbrook. Yuxuan Chen. Hyunsue Kim. Lisa Frammolino. Mengke Liu. Chi-Ruei Pan. Mei-Yin Chou. Chengdong Zhang. and Chih-Kang Shih



ACCESS

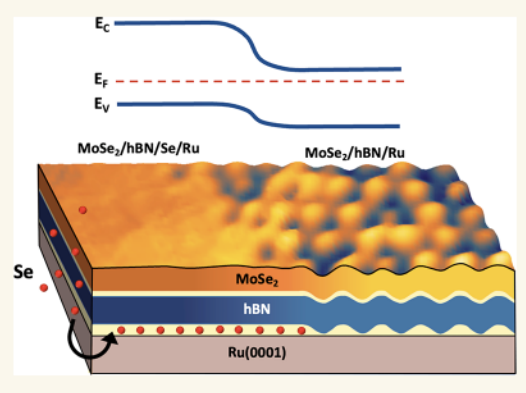
Downloaded via UNIV OF TEXAS AT AUSTIN on May 8, 2024 at 02:07:15 (UTC). See https://pubs.acs.org/sharingguidelines for options on how to legitimately share published articles.

III Metrics & More

Article Recommendations

s Supporting Information

ABSTRACT: The ability to engineer atomically thin nanoscale lateral junctions is critical to lay the foundation for future two-dimensional (2D) device technology. However, the traditional approach to creating a heterojunction by direct growth of a heterostructure of two different materials constrains the available band offsets, and it is still unclear if large built-in potentials are attainable for 2D materials. The electronic properties of atomically thin semiconducting transition metal dichalcogenides (TMDs) are not static, and their exciton binding energy and quasiparticle band gap depend strongly on the proximal environment. Recent studies have shown that this effect can be harnessed to engineer the lateral band profile of a monolayer TMD to create a lateral electronic junction. Here we demonstrate the synthesis of a nanoscale lateral junction in monolayer MoSe₂ by intercalating Se at the interface of an hBN/Ru(0001) substrate. The Se



intercalation creates a spatially abrupt modulation of the local hBN/Ru work function, which is imprinted directly onto an overlying $MoSe_2$ monolayer to create a lateral junction with a large built-in potential of 0.83 0.06 eV. We spatially resolve the $MoSe_2$ band profile and work function using scanning tunneling spectroscopy to map out the nanoscale depletion region. The Se intercalation also modifies the dielectric environment, influencing the local band gap renormalization and increasing the $MoSe_2$ band gap by ~ 0.26 0.1 eV. This work illustrates that environmental proximity engineering provides a robust method to indirectly manipulate the band profile of 2D materials outside the limits of their intrinsic properties.

KEYWORDS: 2D electronic materials. transition metal dichalcogenide. intercalation. environmental engineering. scanning tunneling microscopy

s technology has advanced, the rush to miniaturization has led to the ultimate limit of atomically thin, twodimensional materials. Within this family of materials, the emergence of 2D semiconducting transition metal dichalcogenides (TMDs) has provided exciting possibilities for advanced 2D electronics, including devices comprised of a single atomic layer.1 However, future technology based on TMDs hinges on the capability of creating nanoscale lateral junctions with large built-in potentials. Following the paradigm of three-dimensional counterparts, lateral heterojunctions have been directly synthesized by laterally stitching two different TMD monolayers together,²⁻⁵ although the built-in potentials are on the order of hundreds of meV, limited by the TMD library. 6 Development of substitutional doping is challenging to spatially control while avoiding degradation due to the atomic thin nature of TMDs. However, TMDs are not limited to the toolbox of techniques conventionally used for bulk materials, as their extreme 2D nature provides other modes to

manipulate their electronic properties. A variety of effects modify TMD electronic structure including (but not limited to) surface adsorbates,⁷ substrate hybridization,^{8–10} substrate work function,^{11–13} and dielectric screening.^{14–17} Although this strong influence of the proximal environment creates design challenges, it can also be exploited as a tool to noninvasively engineer a lateral electronic junction in a monolayer TMD. Recently, TMD lateral heterojunctions were "coulomb engineered" by creating an abrupt change in the dielectric environment to modify the local band gap

Received: February 5, 2023 Accepted: March 15, 2023 Published: March 22, 2023





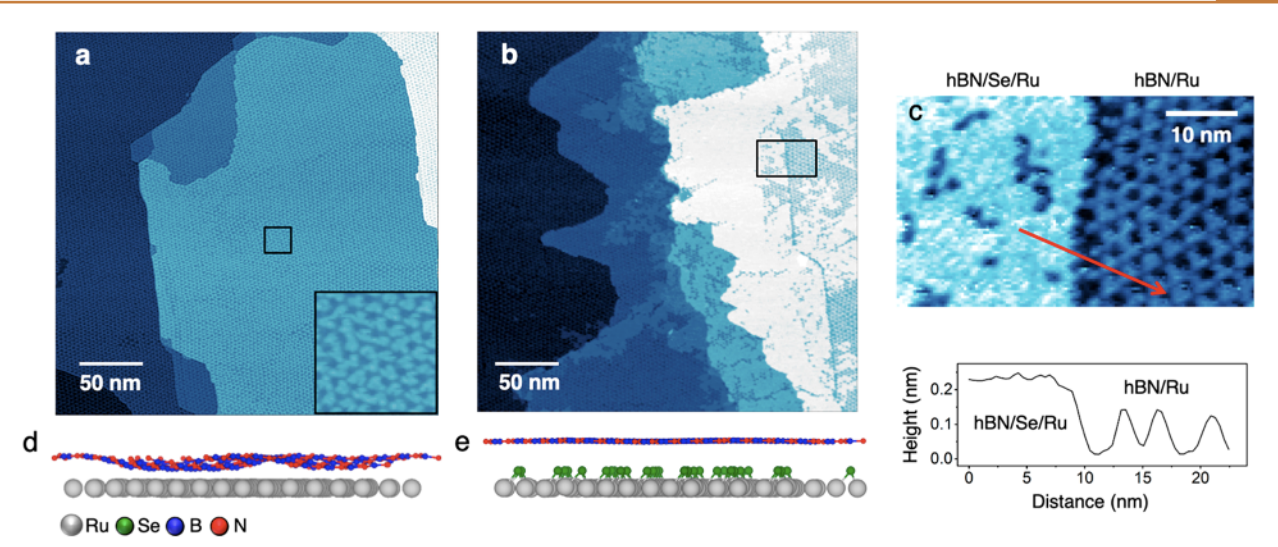


Figure 1. (a) Topographic STM image of hBN on Ru showing a corrugated structure (inset). (b) STM image of the hBN layer after Se intercalation, showing domains of a flat structure have emerged. (c) STM image of a Se intercalation interface similar to the area indicated by the box in (b). To the right is a topographic line cut corresponding to the red vector. (d, e) Side view of simulated hBN/Ru(0001) and hBN/Se/Ru(0001) with a concentration of $33 \boxtimes$ Se (1/3 ML coverage of hcp sites) intercalation, respectively. The STM images in (a), (b), and (c) were obtained at a sample bias of -2 V and tunneling current of 10 pA.

renormalization, though the built-in potentials are relatively small, and the lateral length of the junction is unclear. ^{18–20} The term "heterojunction" was used in prior work to represent the change in band gap, although the junction is formed in the same TMD monolayer; thus we use the more general term "electronic junction". Similarly, lateral junctions were engineered by utilizing surface adsorbates and ferroelectrics to electrostatically tune the Fermi level position and work function. ^{7,21,22} The above examples illustrate that environmental proximity engineering is a promising direction for future TMD lateral electronic junction design and invite further exploration.

Here we create a nanoscale lateral junction in a single MoSe₂ layer with a built-in potential of 0.83 ± 0.06 eV, utilizing a proximity engineering approach that centers on Se intercalation at the interface of an hBN/Ru(0001) heterostructure substrate. The interaction of hexagonal boron nitride (hBN) grown epitaxially on transition metal substrates such as Ru(0001) produces a so-called corrugated "nanomesh" superstructure that exhibits a periodic modulation of the work function. 23,24 It was later shown that this modulation translates directly to a corresponding periodic shift of ~0.15 eV of the band profile of a MoSe₂ monolayer epitaxially grown on top of the hBN/Ru(0001), signifying a purely electrostatic effect. 11 Although hBN is normally a wide band gap insulator, the MoSe₂ on hBN/Ru(0001) also interestingly exhibits a smaller band gap than on graphite or graphene, suggesting a larger band gap renormalization due to the strong interaction between the hBN and Ru.11 It is well established that intercalation of adsorbates alters the interaction between hBN on transition metal substrates by electronically decoupling the hBN layer, resulting in a large enhancement of the work function. 25-29 These prior studies provide the framework to develop a strategy to engineer a nanoscale lateral junction with a large built-in potential by utilizing Se intercalation of an hBN/Ru platform to create an underlying electrostatic template that is imprinted on overlying MoSe₂. Here we examine the relationship of the work function modulation,

substrate dielectric screening, and MoSe₂ band profile at the nanoscale.

RESULTS AND DISCUSSION

The hBN/Ru platform is synthesized using the welldocumented ultra-high-vacuum (UHV) chemical vapor deposition (CVD) technique (see Methods for details), and the resulting high quality hBN monolayer (see Figure 1a) shows the distinct corrugated superstructure as was previously reported.^{24,30} Se intercalation is achieved by exposing the corrugated hBN/Ru to Se vapor in a molecular beam epitaxy system (see Methods), which changes the hBN surface morphology. As shown in Figure 1b, large flat regions emerge where the Se has intercalated into the hBN/Ru interface. Figure 1c allows closer inspection of an hBN intercalation boundary with a corresponding topographic profile that shows the apparent height of the hBN increases as the Se intercalant decouples the hBN from the Ru. We performed a firstprinciples calculation of the Se intercalation between the hBN and Ru substrate with a range of concentration from 11 (1/9 ML) to 100∅ (1 ML). We found that upon Se intercalation, regardless of the Se concentration, the corrugated hBN is decoupled from the Ru, which increases the average interlayer distance and transforms hBN to an almost flat layer (see Supporting Information). We obtained the intercalation energy from density functional theory (DFT) as a function of the average coverage and performed stability analysis for various intercalated phases. Our analysis suggests that with the observed coexistence of the pristine and Se intercalated regions, a Se concentration of $25 \boxtimes \le x \le 33 \boxtimes$ is most likely (see Supporting Information). However, we note that there is a large range of concentration with similar stability; therefore the Se intercalation is likely inhomogeneous, as supported by our low-energy electron diffraction (LEED) measurements (see Supporting Information). Our STM measurements further show that the Se intercalation increases the hBN work function by 0.85 ± 0.1 eV, which we discuss below. We note that this change in the work function and surface morphology is a common phenomenon for intercalated hBN on other

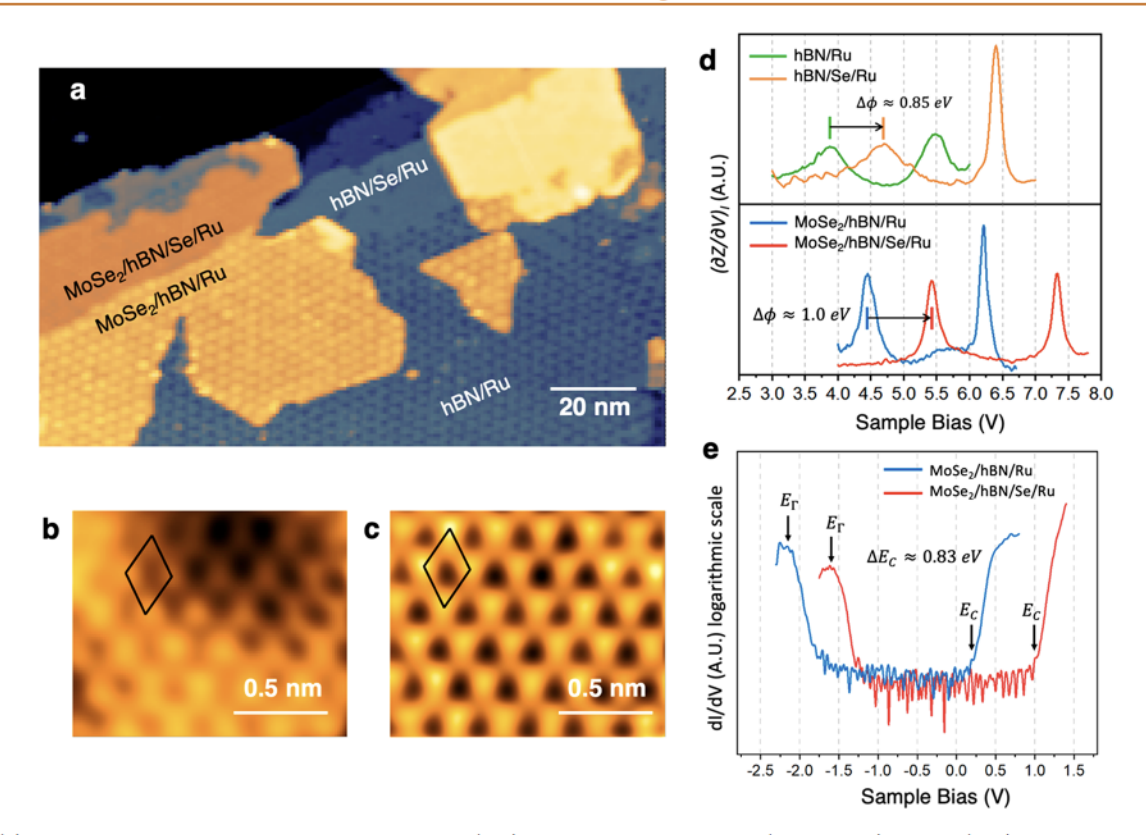


Figure 2. (a) STM image of MoSe₂ on Se-intercalated hBN (flat) and unintercalated hBN (corrugated) on Ru. (b, c) Atomic resolution STM images of the corrugated MoSe₂ on hBN/Ru and flat MoSe₂ on hBN/Se/Ru, respectively. (d) dZ/dV FER spectroscopy on hBN/Ru (green) and hBN/Se/Ru (orange) (top) and on the MoSe₂/hBN/Ru (blue) and Se-intercalated MoSe₂/hBN/Se/Ru (red) (bottom). We note that the measurements on the MoSe₂/hBN/Ru and hBN/Ru were taken on the "wire" regions of the corrugated superstructure reported in ref 11. (e) d \boxtimes /dV spectroscopy averaged from different locations on MoSe₂/hBN/Ru at "wire" regions (blue) and Se-intercalated MoSe₂/hBN/Se/Ru (red). STM images obtained at a sample bias and current set point of (a) V = -2.6 V, $\boxtimes = 5$ pA, (b) V = -1.3 V, $\boxtimes = 0.25$ nA, and (c) V = -1.3 V, $\boxtimes = 20$ pA.

transition metal substrates, suggesting that this approach may be generalized. $^{25-28}$

The epitaxial MoSe₂ synthesis and Se intercalation are achieved with a direct one-step method by applying a high Se overpressure during the MoSe₂ growth (see Methods). An STM topographic image of the heterostructure (Figure 2a) shows the coexistence of two structural phases, flat and corrugated, of both the MoSe₂ and the underlying hBN (see Supporting Information for an analysis of MoSe₂ growth). The growth of the hBN on Ru is self-limited to a monolayer (as shown by Figure 1a); 11,24 therefore islands on the hBN surface can be attributed to the MoSe₂ (shown in orange in Figure 2a). We note that the flat hBN/Se/Ru regions often lie next to the flat MoSe₂, showing a continuation of the Se intercalation. Thus, the overlying MoSe₂ mirrors the structural changes of the hBN, appearing flat in the Se intercalated regions, as shown by the atomic resolution STM images of the MoSe₂ surface (Figure 2b,c). From atomic resolution STM images, we measure a MoSe₂ lattice constant of 0.33 \pm 0.01 nm, further confirming that the islands are indeed MoSe₂ (see Supporting Information). The Se intercalation is often concentrated to the Ru step edges, creating a long and straight intercalation boundary with a sharp interface (see Figure 2a). The abrupt transition from the flat to corrugated morphology hints that the MoSe2 electronic structure evolves over the same length scale, as discussed later.

Next, we investigate how the Se intercalation of the hBN influences the electronic structure of the MoSe₂ overlayer.

Shown in Figure 2d are $(\partial Z/\partial V)_I$ spectra acquired in the constant current mode revealing field emission resonances (FER) obtained on hBN/Ru and hBN/Se/Ru regions, respectively. The onset of the first resonance of the FER spectrum is a good approximation for the sample work function^{31,32} (discussed in the Supporting Information); therefore a change in the onset bias reflects a relative change in the work function. Figure 2d shows that upon Se intercalation of the hBN/Ru, the work function is increased by 0.85 ± 0.1 eV, recovering a value similar to that of clean Ru. Our DFT calculations show a consistent work function increase of 1.05 ± 0.07 eV for intercalant concentration ranging from 11 to 33 (see Supporting Information). Thus, there is a range of stable Se concentrations (as discussed above) that give a similar work function change; we suggest that the exact Se composition is not critical and is likely inhomogeneous. Similar experimental studies of intercalated hBN on transition metals have shown that the decoupling occurs at some critical intercalant coverage and further intercalant exposure does not alter the hBN electronic properties. 25,27 Similar to previous reports for other intercalants of hBN/Ru,²⁶ this implies that the increase in work function is governed by the isolation of the hBN, which disrupts the strong charge transfer with the Ru, and is insensitive to the detailed Se structure. Interestingly, FER measurements on the epitaxially grown MoSe₂ monolayers show a similar work function increase (Figure 2d bottom) due to the Se intercalation, signifying that the changes in

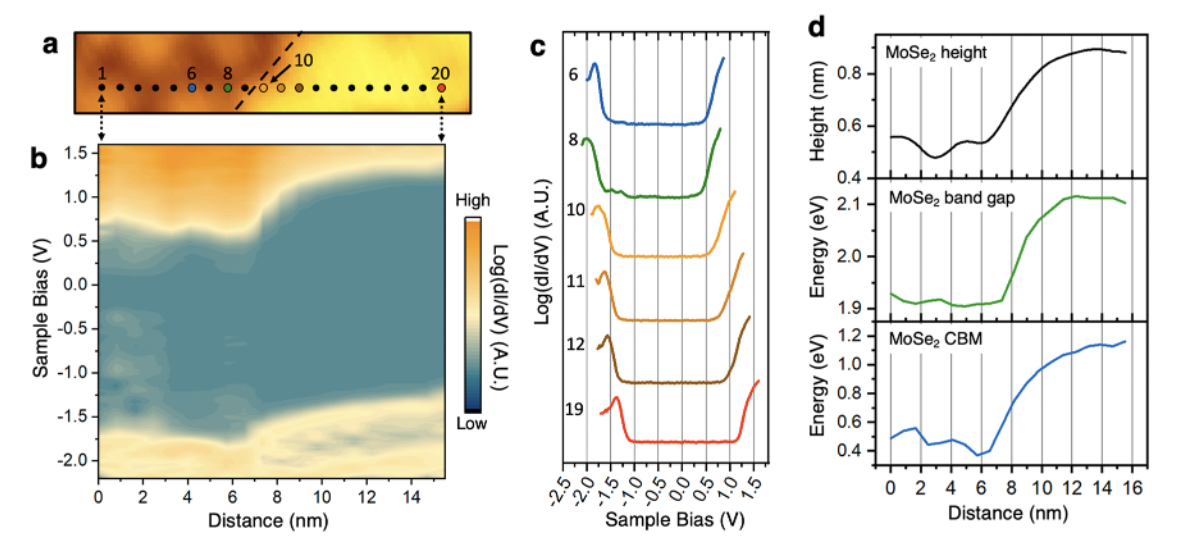


Figure 3. (a) STM image of an intercalation interface between the $MoSe_2/hBN/Ru$ and $MoSe_2/hBN/Se/Ru$ obtained at a sample bias of -2 V and current set point of 10 pA. (b) Real space 2D color rendering of $d\mathbb{Z}/dV$ spectroscopy obtained on the points from (a) along a 15.5 nm line. (c) Select spectra from the line indicated in (a), showing the changes in the $MoSe_2$ band gap across the intercalation boundary. (d) Height profile (top), plot of the $MoSe_2$ band gap (middle), and plot of the $MoSe_2$ CBM (bottom) extracted from the spectra in (b).

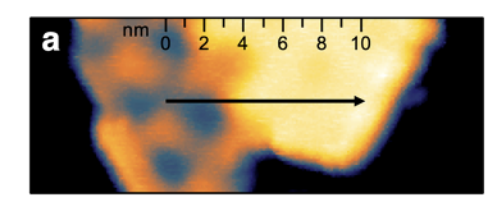
electrostatic potential are mirrored in the $MoSe_2$. A difference of $\Delta\phi$ (\sim 0.15 eV) is likely due to the spatial fluctuation of the intercalation, as the FER of the $MoSe_2$ and that of the hBN are measured at different locations. Due to the modulation of the work function across the corrugated $MoSe_2$ and hBN (discussed above), it is important to note that the FER values reported here correspond to the reported "wire" regions of the corrugated nanomesh reported in ref 11.

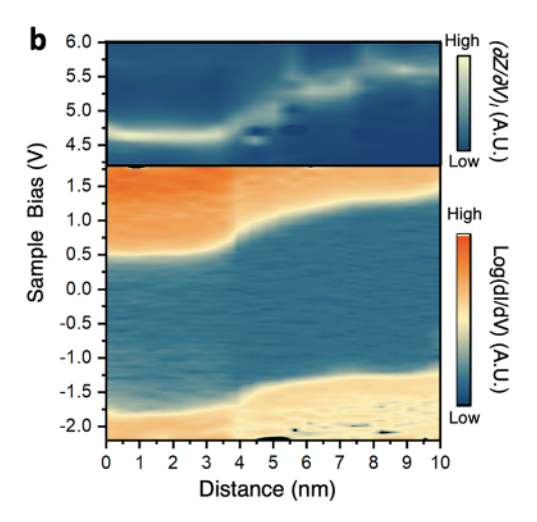
We performed dI/dV tunneling spectroscopy to determine how the Se intercalation changes the band gap of the MoSe₂, as shown in Figure 2e. Averaged conductance spectra obtained on different locations on the intercalated MoSe₂ (red) and wire regions of the corrugated MoSe₂ (blue) show a dramatic shift of the MoSe₂ band gap. Following the method of Ugeda et al. (see ref 14) we determined the conduction band minimum (CBM) positions (black arrows) of the averaged spectra and find that the Se intercalation increases the CBM position by 0.83 ± 0.06 eV. This large upshift in energy is correlated with the increase in the substrate work function (discussed above), which tunes the MoSe₂ band profile via the electrostatic field effect. Taking into account that the valence band maximum (VBM) at the K point is 0.4 eV above the Γ point, ^{14,33} we determine a quasiparticle band gap of ~1.94 eV at the corrugated region, which agrees with the previous reported value, 11 and ~2.2 eV at the Se-intercalated region. This band gap increase hints that the dielectric screening differs between the two regions, leading to a variation in the band gap renormalization. The above analysis underscores the power of Se intercalation as a method to tune the hBN/Ru electrostatic potential landscape, which strongly influences the electronic properties of the overlying MoSe₂ monolayer.

We next answer whether this large built-in potential is supported in the nanoscale regime by examining the detailed spatial evolution of the MoSe₂ band profile. We performed scanning tunneling spectroscopy (STS) dI/dV measurements along a line across the intercalation boundary shown in Figure 3a to spatially resolve the band gap. Figure 3b depicts a 2D color rendering of the real space mapping of the MoSe₂ band profile, exposing an unmistakable nanometer-scale lateral junction. This gives a qualitative view of the band bending

behavior as the color scale does not reflect the band edge locations, which are clarified by the plot of select spectra from the line spectroscopy (Figure 3c). We note that the line cut slightly overlaps the corrugation, resulting in a modulation that shifts the bandgap (Figure 3c spectra 6 blue, 8 green), as was previously reported. 11 Close inspection of the spectra in Figure 3c unveils that the band gap renormalization begins abruptly at the interface (10, yellow) and is complete within a few nanometers (12, brown), while the shift in the band profile continues (19 red). Figure 3d shows a comparison of the MoSe₂ band gap, CBM position, and STM topographic profile along the line cut, elucidating the length scales of the band gap renormalization and the electrostatic shift of the band profile. This analysis shows that the renormalization of the quasiparticle band gap is localized to the intercalation boundary and is complete within ~4 nm (middle panel), while the band bending continues. Recent theoretical investigations of coulomb engineered TMD lateral electronic junctions predicted that band gap renormalization is completed within two unit cells;^{34,35} however, these calculations consider an atomically abrupt dielectric interface. This suggests that the nanometer scale of the MoSe2 band gap renormalization reflects the length scale over which the hBN is decoupled from the Ru.

In order to characterize the spatial relationship between the local work function and the MoSe₂ band profile, we carry out FER $(\partial Z/\partial V)_I$ and STS dI/dV band mapping along the same line across the intercalation interface (Figure 4a black vector). We note that the work function and band gap measurements discussed above (Figure 2) were obtained separately, albeit with the same tip. Thus, we map the work function and band profile in tandem to address possible uncertainty due to spatial inhomogeneity of the intercalation. Figure 4b depicts a 2D color mapping of the spatially resolved FER $(\partial Z/\partial V)_{I}$ (top) and dI/dV spectroscopy (bottom), with a ~ 0.5 nm uncertainty in the alignment due to possible drift between measurements. Although there is some noise in the FER spectra using the same tip, the resulting energy profiles of the first FER peak $\phi(x)$ and the CBM $E_{\rm C}(x)$ show a striking similarity (see Figure 4b top). This qualitatively shows that the MoSe₂ CBM tracks





the work function, affirming that the MoSe₂ band bending is essentially an imprint of the changing electrostatic landscape. This suggests that the electron affinity $= \phi - E_C$ is roughly constant (within experimental error). Note that the band bending of the VBM shows a different dispersion, which we suggest comes from the influence of the band gap renormalization. Theoretical investigations have predicted that band gap renormalization should be symmetric, 18,20,34 and therefore the band gap change should be split evenly between the valence and conduction bands when referenced from the vacuum level. Our measurements suggest that this might not be the case, as symmetric band gap renormalization should result in a variation in . However, we note that better energy resolution is necessary to definitively draw this conclusion, and more experimental and theoretical investigations are necessary to tease apart the complexity of the underlying physical phenomena at play.

CONCLUSIONS

In conclusion, this study confirms that environmental proximity engineering is a powerful method to noninvasively create a nanoscale, planar, lateral electrostatic junction by coupling a TMD monolayer with a nanostructured electrostatic potential template. We show that intercalation can be used as a tool to create electronic junctions by utilizing a facile approach of all UHV *in situ* epitaxial growth and intercalation with Se vapor. We further mapped the band profile, band gap renormalization, and work function of the MoSe₂ junction at the nanoscale using STM/S, giving a complete spatial characterization of their relationships. This characterization reveals that the junction has a built-in potential of nearly 1 eV at the nanometer length scale, larger than previously reported TMD lateral junctions, ^{3,20,21} which suggests the possibility of devices that can function at room temperature. In addition to

enabling the creation of an ultranarrow junction, this approach further minimizes the effect of dopant scattering. This demonstration of a nanoscale lateral junction is surprising in light of a previous theoretical analysis that predicts that the depletion region for a doped p-n junction is significantly wider for 2D electronic junctions than that of 3D counterparts. 30 Thus, the creation of a nanoscale junction with a builtin potential of ~0.83 eV exemplifies that proximity engineering can expand the limits of attainable band profiles for TMDbased devices. In fact, work function shifts greater than 2 eV have been demonstrated for other hBN/intercalant/substrate systems,³⁷ indicating that even larger built-in potentials are most likely achievable. We expect this approach is not limited to the scope of hBN/TM templates and can be generalized to any substrate or capping layer with nanostructured electrostatic properties, inviting further exploration for nanoscale devices based on atomically thin semiconductors.

METHODS

Growth and Intercalation of MoSe₂/hBN/Ru Heterostructures. A clean Ru(0001) surface was prepared by sputtering a Ru single crystal with Ar+ and annealing at 1000 °C in repeated cycles (1.5 kV, 5×10^{-5} Torr Ar). A monolayer of hBN was epitaxially grown on the Ru by leaking a borazine (H₆B₃N₃) precursor vapor into a UHV chamber at a pressure of 1×10^{-7} Torr for 5 min while the Ru was held at 1000 °C, then slowly lowered to room temperature. The quality of the hBN was checked by in situ STM and LEED measurements. The hBN/Ru was transferred in situ to an MBE chamber for the intercalation and MoSe2 growth. To prepare the intercalated hBN/Ru sample, an effusion cell with Se was used to deposit Se at a rate of 0.6 nm/min on the hBN surface, at a pressure of 1×10^{-9} Torr (the chamber base pressure is 3×10^{-10} Torr) for 60 min. The sample was maintained at a temperature of 480 °C during the deposition, followed by a 30 min anneal at the same temperature. The MoSe₂ growth was performed in the same chamber with an ebeam evaporation of high-purity Mo (99.95□) and effusion of Se (99.999M) sources at a ratio of 1:30. A hBN/Ru sample was maintained at 410 °C for a growth of 55 min; then the temperature of the Mo source was decreased while the evaporation of the Se continued. The sample was annealed in the Se vapor at the growth temperature for an additional 15 min. We note that the intercalated MoSe₂/hBN/Ru sample was achieved by growing the MoSe₂ on an hBN/Ru substrate that was not Se intercalated beforehand; the intercalation occurred during the growth and anneal of the MoSe2.

Scanning Tunneling Microscopy and Spectroscopy. All STM measurements reported here were acquired at a temperature of 77 K in UHV (chamber base pressure was below 5×10^{-11} Torr). Electrochemically etched tungsten tips were cleaned by a UHV electron bombardment treatment. A home-built STM was used, and the bias was applied to the sample. The dI/dV spectra were taken with a constant tip to sample distance while the feedback was turned off. The dZ/dV spectra were acquired with the feedback on and the tip sample distance Z changing to maintain a constant current during the bias sweep.

ASSOCIATED CONTENT

Supporting Information

The Supporting Information is available free of charge at https://pubs.acs.org/doi/10.1021/acsnano.3c01082.

First-principles calculation of the intercalated hBN/Se/Ru, low-energy electron diffraction measurements of the Se-intercalated hBN/Ru, analysis of the STM topography of the MoSe₂ on Se-intercalated hBN/Ru, measuring the lattice constant of the MoSe₂, and determining the work function with field emission resonance spectroscopy (PDF)